Astronomical and Astrophysical Transactions (*AApTr*), 2026, Vol. 36, Issue 1, pp. 9–18,
ISSN 1055-6796, Photocopying permitted by license only, ©Cambridge Scientific Publishers

Force-free magnetic flux ropes as active flare elements on the Sun

A.A. Solov'ev, O.A. Korolkova*, E.A. Kirichek

Main (Pulkovo) Astronomical Observatory of RAS, Saint-Petersburg, Russia

Received 9 January, 2026; accepted 31 January, 2026

Solar and stellar flares apparently have a common physical nature, differing mainly in their energy scales. The basic current-carrying structures on the Sun and stars are twisted magnetic loops, or magnetic flux ropes. Owing to the tenuousness of stellar atmospheres, the magnetic fields of such flux ropes possess a force-free structure. Models of force-free ropes differ in their internal current distributions: in some cases, strong electric currents are concentrated along the rope axis, whereas in others they are confined to a thin peripheral shell. However, there exists a third type of force-free magnetic flux rope, in which electric currents are concentrated near a magnetic surface where their direction changes sign. In this paper, we analyze a new model of force-free flux ropes of this third type.

All force-free magnetic flux ropes share a common physical property that can trigger flare energy release. As the apex of a loop-shaped rope rises into the rarefied solar corona, the external pressure that prevents its lateral expansion steadily decreases. When this pressure drops below a critical value, the longitudinal magnetic field tends to zero at the current inversion surface. At this stage, the azimuthal current j_φ and the force-free parameter α, which approach a discontinuity at this surface, grow rapidly in its vicinity. This process leads to the excitation of ion-acoustic plasma instability, a sharp reduction in plasma conductivity, rapid dissipation of magnetic fields and currents within the rope, and the generation of strong super-Dreicer electric fields. The combination of these effects, together with the Parker effect – namely, the redistribution of torque along the rope axis at the Alfvén speed, resulting in discrete peaks of flare radiation – provides a consistent explanation of the main observational features of solar flares.

Keywords: Magnetic fields – plasmas – instabilities – Sun: flares – Sun: corona – magnetohydrodynamics (MHD)

1 Introduction

Solar flares are among the most striking and powerful geoeffective manifestations of solar activity, with total energies reaching 10^{32} erg. The principal current-carrying

*Email: korolkova@gaoran.ru

magnetic structures both on the Sun and in stellar atmospheres are twisted magnetic flux tubes, or magnetic flux ropes. Because stellar atmospheres are highly rarefied, the magnetic fields in such flux ropes generally adopt a force-free configuration (Parker, 1979; Priest, Forbes, 2000; Artsimovich, Sagdeev, 1979; Parker, 2007; Shafranov, 1963).

Despite the considerable progress achieved in observational and theoretical studies of solar flares, the physical mechanisms responsible for the rapid conversion of magnetic energy into plasma heating and particle acceleration remain under active investigation. In particular, the relative roles of magnetic reconnection and current dissipation in strongly twisted magnetic structures are not yet fully understood.

In the framework of the so-called standard flare model, flare energy release is usually attributed to magnetic reconnection in current sheets formed during the rapid reconfiguration of coronal magnetic fields. This paradigm has been extensively developed and successfully applied to a wide range of observational manifestations of solar flares, including impulsive energy release, particle acceleration, and post-flare loop formation (e.g., Priest, Forbes 2000).

At the same time, it is well known that current sheets are intrinsically unstable and tend to fragment into a hierarchy of magnetic islands and localized dissipation regions. Such fragmentation strongly limits the lateral inflow of fresh magnetic flux and may restrict both the efficiency and duration of energy release (Artsimovich, Sagdeev, 1979). This fundamental difficulty was already clearly recognized in the late 1970s (see, for example, Fig. 2.31 in Artsimovich, Sagdeev 1979, p. 208), which illustrates the resonant destruction of magnetic surfaces in a neutral current sheet and the resulting stochastic motion of magnetic field lines.

Nevertheless magnetic reconnection remains the dominant framework used to interpret solar and stellar flare phenomena.

Recent high-resolution observations emphasize the importance of flux-rope structure in flare onset and energy release. Strongly sheared twisted structures above the polarity inversion line (PIL) host narrow channels of plasma heating and electron acceleration, suggesting that reconnection can operate within and between twisted flux elements, combining reconnective and ideal processes (Sharykin et al., 2018, 2020). Statistical studies further indicate that the pre-flare evolution of flux ropes and PIL current distributions correlates with flare strength and timing (Sharykin et al., 2020; Schrijver, 2009). Large-scale reviews highlight that flare energetics depend on flux-rope evolution, field topology, and current systems, not only on reconnection in current sheets (Schrijver, 2009).

Using nonlinear force-free field (NLFFF) extrapolations and the virial theorem, Livshits et al. (2015) estimate the free magnetic energy above active regions, showing that solar flares typically do not exceed $\sim 3 \times 10^{32}$ erg, while solar-type flares on G stars may reach $\sim 10^{34}$ erg. Stellar flares with energies up to $\sim 10^{36}$ erg likely involve fundamentally different processes. The similarity between solar and stellar activity cycles, and the scaling of flare properties with stellar magnetic activity, suggests that stronger twisting and longer magnetic loops in stars underpin these extreme events (Obridko et al., 2023).

In this sense, force-free magnetic flux ropes should be regarded as active flare elements capable of accumulating substantial amounts of free magnetic energy due to field twisting, both in solar and stellar coronae. The mechanism introduced in this

paper can complement the reconnection process, acting alongside it to enhance the efficiency and speed of energy release within flaring structures.

Crucially, flare energy can also be released independently of reconnection, occurring directly within sufficiently tightly twisted magnetic flux tubes when conditions favor the onset of internal plasma instabilities.

In our work we have identified a new property of force-free magnetic flux ropes: when the external pressure that prevents their lateral expansion decreases below a certain threshold, conditions arise within the rope for the excitation of plasma turbulence and rapid energy release (Solov'ev, Kirichek, 2021; Solov'ev, 2022, 2024; Solov'ev, Kirichek, 2024; Solov'ev, 2025).

On the Sun, magnetic filaments that form over relatively short time scales have a finite transverse size a, which limits the spatial extent of their magnetic fields. If the magnetic field of such a filament is twisted, then on its lateral surface, $r = a$, the azimuthal magnetic field necessarily vanishes, $B_\varphi(a) = 0$. Consequently, the total longitudinal electric current flowing along the filament axis z is zero, $I = \int_0^a j_z 2\pi r dr = \frac{c}{4\pi}\int_0^a \left(\frac{1}{r}\frac{\partial}{\partial r} r B_\varphi\right) 2\pi r dr = \frac{c}{2} r B_\varphi(r)|_0^a = 0$, so that the forward current near the axis is exactly compensated by the return current at the periphery. Configurations of this type are referred to as *current-shielded*. Unshielded electric currents cannot exist in a conducting plasma (Parker, 1979; Priest, Forbes, 2000; Artsimovich, Sagdeev, 1979; Parker, 2007; Shafranov, 1963; Solov'ev, Kirichek, 2021).

The magnetic fields of flare-associated filaments must be sufficiently strong (on average, exceeding ~ 200 G) to account for the observed flare energies. As a result, the magnetic field inside such ropes possesses a force-free structure,

$$[\nabla \times \mathbf{B}] = \alpha(\mathbf{r})\,\mathbf{B}, \qquad \nabla\alpha(\mathbf{r}) \cdot \mathbf{B} = 0, \tag{1}$$

where α is a pseudo-scalar function of spatial coordinates. In force-free magnetic flux ropes, electric currents flow strictly along magnetic field lines.

Force-free magnetic flux ropes may exhibit different internal current distributions. In some cases, strong currents are concentrated along the rope axis (Solov'ev, 2022, 2024), whereas in others they are confined to a thin peripheral shell (Solov'ev, Kirichek, 2024). In this paper, we consider a new class of force-free magnetic flux ropes in which electric currents are absent both at the axis and at the lateral boundary of the rope, but are instead concentrated within its interior, near a magnetic surface where the current changes sign (Figure 1). We refer to this surface as the *current inversion surface* (CIS).

We emphasize that the flare energy-release mechanism identified here operates in essentially the same manner for any internal current structure of a force-free magnetic flux rope.

2 Model of magnetic flux rope

Let us consider the equilibrium of a horizontal magnetic filament embedded in a plane-parallel hydrostatic atmosphere (Figure 1). On the lateral surface $r = a$, where the azimuthal magnetic field vanishes $B_\varphi(ka) \to 0$, the longitudinal magnetic field

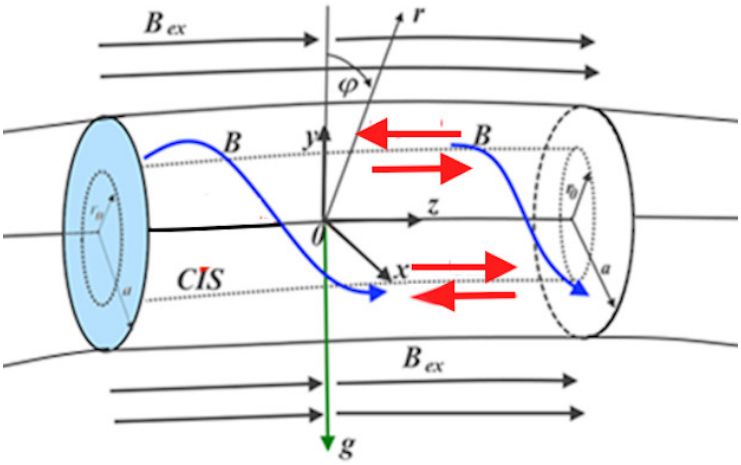


Figure 1 A section of a shielded magnetic flux rope of radius a. The electric current (red arrows) is zero at the axis and at the edge of the flux rope, and changes sign at a distance kr_0 from the axis, on the CIS (current inversion surface). Cartesian and cylindrical coordinate systems are shown, and $B_{\rm ex}$ is the external field holding the flux rope in lateral equilibrium.

continuously transforms into an external field $B_z(ka) \to B_{z,\rm ex}$, which, according to Shafranov's theorem (Shafranov, 1963), prevents the flux rope from expanding to infinity.

We assume, following Parker (1979), axial and translational symmetries. The z-axis is directed along the filament axis, the x-axis is directed across the filament, and the y-axis is directed vertically upward, measured from the magnetic axis of the rope. The gravitational force is $\mathbf{F_g} = -\rho(y) g \mathbf{e_y}$, where ρ is the gas density. Under conditions of magnetohydrostatic equilibrium, the force balance equation takes the form

$$\frac{1}{4\pi}\left[[\nabla \times \mathbf{B}] \times \mathbf{B}\right] - \nabla P + \rho g \mathbf{e_y} = 0. \tag{2}$$

This equation must be supplemented by the solenoidal condition $\nabla \cdot \mathbf{B} = 0$, and by the ideal gas equation of state, $P = \rho R T \mu^{-1}$, where $\mathbf{B}$ is the magnetic induction, P is the gas pressure, T is the plasma temperature, and μ is the mean molecular weight. This system of equations is formally incomplete, since it does not include an energy transport equation. However, this is not essential for the present analysis, which focuses on strong force-free magnetic fields, for which the pressure gradient and all non-magnetic forces can be neglected.

The magnetic field is specified in terms of the magnetic flux function as

$$A(x,y) = \int_0^x B_y(x,y)dx. \tag{3}$$

The transverse components of the magnetic field are therefore given by Landau, Lifshitz (1982) $B_x = -\dfrac{\partial A}{\partial y}$, $B_y = \dfrac{\partial A}{\partial x}$.

In terms of the flux function A, the equilibrium equation (2) can be written in the form (Solov'ev, 2022, 2024; Solov'ev, Kirichek, 2024)

$$\frac{\partial^2 A(x,y)}{\partial x^2} + \frac{\partial^2 A(x,y)}{\partial y^2} = -\frac{1}{2}\frac{dB_z^2(A)}{dA} - 4\pi\frac{\partial P(A,y)}{\partial A}. \tag{4}$$

By specifying the flux function and neglecting the gas pressure term, we obtain an equation for the longitudinal magnetic field inside the rope, which, owing to translational symmetry, depends only on the flux function A. To model the internal current structure of the flux rope, we choose the flux function in the form

$$A(x,y) = B_0 k^{-1}\left[\exp\Big(mk^2\left((x^2+y^2)-(x_0^2+y_0^2)\right)\Big)+q\right]^{-1}. \tag{5}$$

From the geometry of the system it follows that $(kr)^2 = (kx)^2 + (ky)^2$. Here B_0 characterizes the magnetic field strength, k is a scale factor with the dimension of inverse length, and m and q are free parameters that allow one to adjust the amplitude and spatial distribution of electric currents within the rope. The introduction of these parameters is necessary, since solar and stellar flares exhibit a wide range of energies and durations. The azimuthal magnetic field is then readily obtained from the expressions given above $B_\varphi(kr) = 2m\,B_0\,kr\,\exp\left(mk^2(r^2-r_0^2)\right)\Big[\exp\left(mk^2(r^2-r_0^2)\right)+q\Big]^{-2}$.

Below we consider a representative model with $m = 15$ and $q = 5$, which is typical for strong solar flares and adequately reproduces their principal features. The longitudinal magnetic field is obtained by neglecting the gas pressure term in equation (5) and integrating (4) with respect to the flux function A:

$$B_z(kr) = \sqrt{B_{\rm ex}^2 - B_0^2 f(kr)} = B_0\sqrt{G - f(kr)}. \tag{6}$$

Here $G = B_{\rm ex}^2 B_0^{-2}$. We emphasize that the external field, which prevents the rope from lateral expansion, arises here not as an additional boundary condition imposed to satisfy Shafranov's theorem, but as a natural nonzero constant of integration.

For $m = 15$ and $q = 5$, the function $f(kr)$ entering equation (6) has the explicit form.

The behavior of the field $B_z(kr)$ is shown in Figure 2. At sufficiently high external pressure, the field exhibits a shallow minimum near the current inversion surface (CIS). As the external pressure decreases and approaches a critical value, the longitudinal magnetic field tends to zero at the CIS. In this regime, the force-free parameter $\alpha(kr)$ grows sharply in the vicinity of the CIS, since it is determined by the relation (Solov'ev, Kirichek, 2021; Solov'ev, 2022) $\alpha(r) = -k\dfrac{3F' + rF'\prime}{4B_zB_\varphi}$, where $F = B_z^2 + B_\varphi^2$ and the primes denote derivatives with respect to kr.

The relationship between the scale factor k and the radius of the rope cross-section at which the electric currents vanish is determined from Figures 2–4 as $ka = 1.8$.

The electric current density components inside the rope are given by the standard expressions (Solov'ev, Kirichek, 2024; Solov'ev, 2025) $j_\varphi(r) = \dfrac{c}{4\pi}\left[\nabla\times\mathbf{B}\right]_\varphi = -\dfrac{ck}{4\pi}\dfrac{\partial B_z}{\partial(kr)}$, $j_z(r) = \dfrac{ck}{4\pi}\left(\dfrac{\partial B_y}{\partial(kx)} - \dfrac{\partial B_x}{\partial(ky)}\right) = \dfrac{ck}{4\pi}\Delta A$. Their radial profiles are shown in Figure 3 in units of $ckB_0(4\pi)^{-1}$.

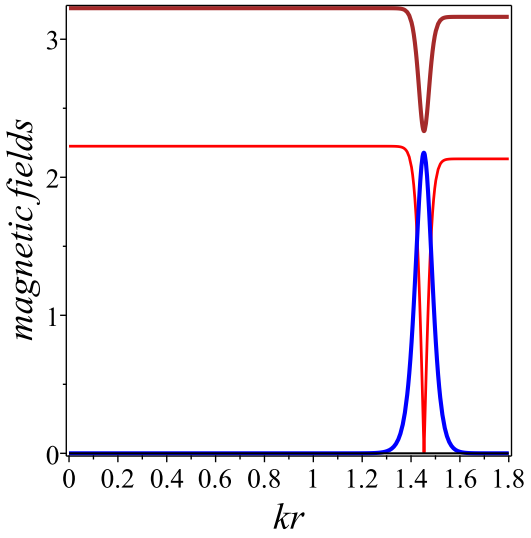


Figure 2 Azimuthal (blue) and longitudinal (red) magnetic fields near the discontinuity at $G = 4.5509 > G_{\rm crit} = 4.550$. The brown curve corresponds to B_z at $G = 2.25 G_{\rm crit}$.

Figure 4 shows the discontinuous behavior of the azimuthal current j_φ and the force-free parameter α when the external pressure reaches its critical value $G_{\rm crit} = 4.550$. As the discontinuity is approached, the electron drift velocity in the vicinity of the CIS inevitably exceeds the ion sound speed. This leads to the excitation of

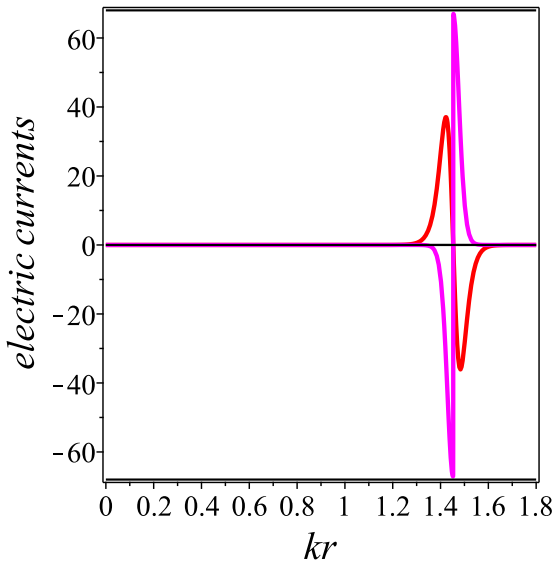


Figure 3 Electric currents in the flux rope near the rupture at $G = 4.5509 > G_{\rm crit=4.550}$. Longitudinal (red) and azimuthal (magenta) current densities are shown in units of $ckB_0(4\pi)^{-1}$.

ion-acoustic instability, which triggers an explosive energy release in the magnetic rope.

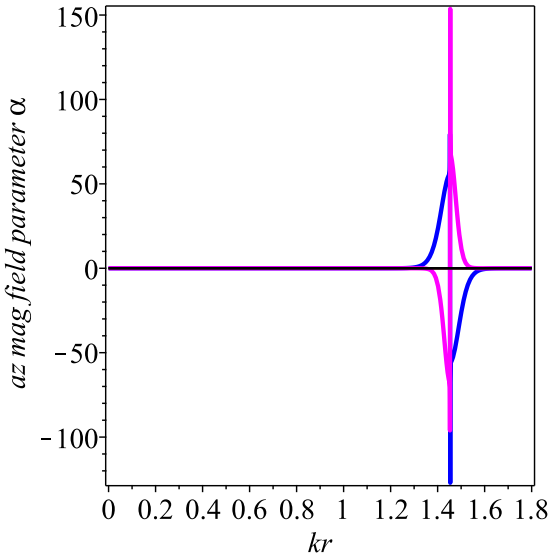


Figure 4 Force-free parameter α near the current inversion surface at $G = 4.5509 > G_{\rm crit} = 4.550$.

3 Plasma instability and energy dissipation

It is well known that the development of ion-acoustic instability requires a non-isothermal plasma, $T_{\rm e} \gg T_{\rm i}$. This condition is naturally satisfied when a magnetic rope rises from the chromosphere, where the electron temperature is $T_{\rm e} \simeq (1.2\text{–}2.0) \times 10^4$ K, into the solar corona, where $T_{\rm e}^* \sim 10^6$ K. Regardless of the specific mechanism of coronal heating, electrons, being much lighter than ions, acquire thermal energy more rapidly.

The second necessary condition for the excitation of ion-acoustic instability is that the electron drift velocity exceeds the ion sound velocity, $v_{\rm is} = \sqrt{k_{\rm B} T_{\rm e} M^{-1}}$, where $k_{\rm B}$ is the Boltzmann constant and M is the mean ion mass, which, for the solar chemical composition, is $m_{\rm p}\,(0.7({\rm H}) + 4 \cdot 0.28({\rm He}) + 35 \cdot 0.02({\rm Metals})) \simeq 2.52\, m_{\rm p}$.

Let us examine this second condition in more detail. We consider the state of the system in the vicinity of the rupture, when the external pressure has not yet reached its critical value but is already close to it. At the rupture itself, the physical parameters formally diverge, so a quantitative analysis is no longer possible.

The electric current density is given by $j(kr) = n_{\rm e} e V_{\rm dr} = n_{\rm e} e \gamma V_{\rm is}$, where $\gamma = V_{\rm dr}/V_{\rm is}$ is the ratio of the electron drift velocity to the ion sound velocity.

Then, from the condition $ka = 1.8$ and Figure 3, it follows that near the CIS, in a state close to the discontinuity (we denote such quantities with an asterisk), we have: $B_0^* = 1000$ G, $j({\rm CIS}) = 1.8 \cdot 65 \cdot c B_0^* (4\pi a)^{-1} = n_{\rm e}^* e \gamma V_{\rm is}$. Taking into account that

$T_e = 10^6$ K, $n_e^* = 4 \cdot 10^7$ cm^{-3}, $B_{ex} = 1000 \cdot \sqrt{4.5509} = 2130$ G (see Figure 2), and considering that the product $T_e n_e^*$ is proportional to the pressure, which, through the ends of the dissipation region (Figure 1), is equalized with those parts of the tube where turbulence is absent, while the quantity $a^* \sqrt{B_0^*}$ is proportional to the magnetic flux of the longitudinal field, which also does not change during dissipation, we write:

$$\gamma(\mathrm{CIS}) = \frac{1.8 \cdot 65 \cdot c\sqrt{MT_e^*}(B_0^*)^{3/2}\left(\frac{B_0}{B_0^*}\right)^{3/2}\sqrt{\frac{T_e}{T_e^*}}}{4\pi e\sqrt{k_B}\cdot(T_e^* n_e^*)a\sqrt{B_0^*}} \approx 5\left(\frac{B_0}{B_0^*}\right)^{3/2}\sqrt{\frac{T_e}{T_e^*}}. \quad (7)$$

If, in the vicinity of the CIS, in the situation before the discontinuity, $B_0 = B_0^* = 1000$ G and $T_e = T_e^* = 10^6$ K, then the value γ(CIS) is approximately equal to 5, and ion-acoustic instability will inevitably arise. It will sharply reduce the plasma conductivity within a fraction of a second, and this anomalous resistance will lead to plasma heating to typical flare temperatures of (3–4)$\cdot 10^7$ K.

This is how the first peak of flare radiation is formed. A remarkable property of a force-free field is that, under Joule dissipation, its internal structure does not change; only the amplitudes of the magnetic field and currents decrease according to the law (Solov'ev, Kirichek, 2024): $\frac{dB_0(t)}{dt} = -\frac{B_0(t)}{\tau}$, $\tau = \frac{2\pi\sigma_{\mathrm{eff}}}{c^2\alpha^2}$. Here σ_{eff} is the plasma conductivity.

The two quantities on the right-hand side of equation (7) begin to change in opposite directions: the term containing the temperature increases by a factor of 3–6, whereas the term containing B_0 decreases with time by no more than a factor of e. As a result, their ratio increases by approximately a factor of 2. We therefore adopt the estimate γ(CIS) = 10.

With a decrease in B_0 and an expansion of the rope cross-section, the well-known Parker effect (Parker, 1979) arises. The rotational moment (torque), $W = 0.5\int_0^a B_z(r)B_\varphi(r)r^2\,dr \sim B_0^2$, applied to each cross-section of the twisted flux tube, becomes weaker in the energy release region. In equilibrium, it must be the same along the entire length of the tube. Therefore, Alfvén waves begin to transfer the azimuthal magnetic flux into the dissipation region, and the magnetic field structure there is restored with a delay determined by the finite Alfvén speed.

As a result, a second peak of flare radiation follows. This process is repeated several times until the free magnetic energy stored in the entire magnetic loop is substantially exhausted.

Let us estimate the energy dissipation time in a force-free flux rope. If $\alpha = (a\sqrt{2})^{-1}$, one obtains the classical expression for the magnetic field dissipation time on a spatial scale a: $\tau = 4\pi\sigma_{\mathrm{eff}}a^{-2}c^{-2}$. However, in force-free flux ropes the parameter α is, as a rule, much larger than the inverse radius. In our model (Figure 5), $\alpha(CIS) = 56 \cdot a^{-1}$, and $\tau = \sigma_{\mathrm{eff}}a^2(500)^{-1}c^{-2}$; thus, the dissipation time decreases by more than three orders of magnitude.

For plasma conductivity in the presence of developed ion-acoustic turbulence, we have (Solov'ev, Kirichek, 2024): $\sigma_{\mathrm{eff}} = 4.53 \cdot 10^4\gamma^{-1}\sqrt{n_e}$. Using this expression, we find that the characteristic dissipation time of magnetic energy in this model (corresponding to the duration of a single peak) is about 15 s, while the total flare energy release time is approximately $7 \times 15 = 105$ s. In the flare of 7 June 1980,

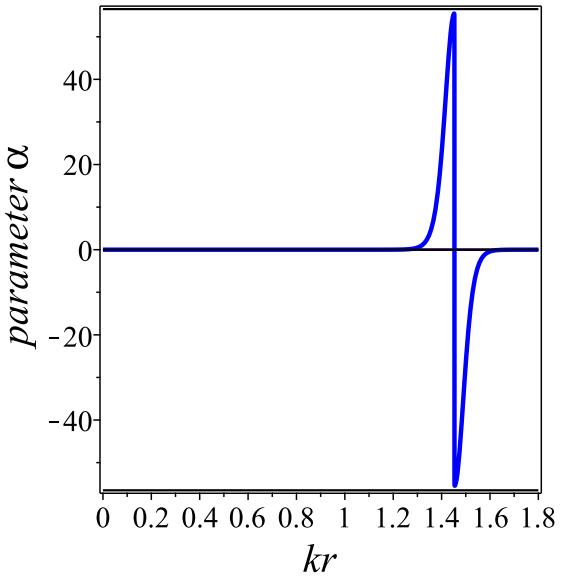


Figure 5 Azimuthal magnetic field (magenta) and force-free parameter (blue) at the critical external pressure $G = G_{\rm crit} = 4.550$, corresponding to the rupture state.

seven distinct radiation peaks were observed over a wide range of wavelengths, from X-rays to microwaves (Kane et al., 1983), which is fully consistent with the properties of large solar flares.

4 Conclusion

Force-free magnetic flux ropes are active flare-producing structures capable of storing large amounts of free magnetic energy through magnetic field twisting, both in solar and stellar plasmas. All such structures share a common property that triggers flare activity: when a flux rope enters the rarefied corona, conditions arise for the development of ion-acoustic plasma turbulence and, consequently, anomalous electrical resistance. Owing to the reduced plasma conductivity and the strong spatial concentration of electric currents within the body of the rope, the magnetic energy dissipation time decreases sharply, reaching values consistent with observations.

The authors declare no conflicts of interest.

References

Artsimovich L.A., Sagdeev R.Z. (1979) Plasma physics for physicists, Moscow: Atomizdat

Kane S.R., Kai K., Kosugi T. et al. (1983) ApJ 271, 376
Landau L.D., Lifshitz E.M. (1984) Course of theoretical physics, Vol. 8: Electrodynamics of continuous media, Oxford: Pergamon Press (Moscow: Nauka, 1982)
Livshits M.A., Rudenko G.V., Katsova M.M. et al. (2015) Adv. Space Res. 55, 3, p. 920
Obridko V.N., et al. (2023) ARep 67, 12, p. 1442
Parker E.N. (1979) Cosmical magnetic fields. Part 1, Oxford: Clarendon Press
Parker E.N. (2007) Conversations on electric and magnetic fields in the cosmos, Princeton, NJ: Princeton Univ. Press
Priest E., Forbes T. (2000) Magnetic reconnection, Cambridge: Cambridge Univ. Press
Shafranov V.D. (1963) in: Problems of plasma theory, No. 2, Moscow: Atomizdat, p. 92
Sharykin I.N., Zimovets I.V., Myshyakov I.I. et al. (2018) ApJ 864, 156
Sharykin I.N., Zimovets I.V., Myshyakov I.I. (2020) ApJ 893, 159
Schrijver C.J. (2009) Adv. Space Res. 43, 5, p. 739
Solov'ev A.A., Kirichek E.A. (2021) MNRAS 505, 3, p. 4406
Solov'ev A.A. (2022) MNRAS 515, 4, p. 4981
Solov'ev A.A. (2024) ARep 101, 6, p. 565
Solov'ev A.A., Kirichek E.A. (2024) AstL 51, 9, p. 50
Solov'ev A.A. (2025) AZh 102, 9, p. 79